

# NIH RELAIS Document Delivery

NIH-10286732

JEFFDUYN

NIH -- W1 MA34IF

JOZEF DUYN  
10 Center Dirve  
Bldg. 10/Rm.1L07  
Bethesda, MD 20892-1150

ATTN: SUBMITTED: 2002-08-29 17:22:17  
PHONE: 301-594-7305 PRINTED: 2002-09-03 07:23:02  
FAX: - REQUEST NO.: NIH-10286732  
E-MAIL: SENT VIA: LOAN DOC  
7967409

---

NIH	Fiche to Paper	Journal
TITLE:	MAGNETIC RESONANCE IN MEDICINE : OFFICIAL JOURNAL OF THE SOCIETY OF MAGNETIC RESONANCE IN MEDICINE / SOCIETY OF MAGNETIC RESONANCE IN MEDICINE	
PUBLISHER/PLACE:	Wiley-Liss, Inc., a division of John Wil New York, NY :	
VOLUME/ISSUE/PAGES:	1996 Oct;36(4):620-6 620-6	
DATE:	1996	
AUTHOR OF ARTICLE:	Yang Y; Glover GH; van Gelderen P; Mattay VS; Santha AK; Sex	
TITLE OF ARTICLE:	Fast 3D functional magnetic resonance imaging at 1	
ISSN:	0740-3194	
OTHER NOS/LETTERS:	Library reports holding volume or year 8505245 8892216	
SOURCE:	PubMed	
CALL NUMBER:	W1 MA34IF	
REQUESTER INFO:	JEFFDUYN	
DELIVERY:	E-mail: jhd@helix.nih.gov	
REPLY:	Mail:	

NOTICE: THIS MATERIAL MAY BE PROTECTED BY COPYRIGHT LAW (TITLE 17, U.S. CODE)

---National-Institutes-of-Health,-Bethesda,-MD-----

# Fast 3D Functional Magnetic Resonance Imaging at 1.5 T with Spiral Acquisition

Yihong Yang, Gary H. Glover, Peter van Gelderen, Venkata S. Mattay, Attanagoda K. S. Santha, Roy H. Sexton, Nick F. Ramsey, Chrit T. W. Moonen, Daniel R. Weinberger, Joseph A. Frank, Jeff H. Duyn

**A new method to perform rapid 3D fMRI in human brain is introduced and evaluated in normal subjects, on a standard clinical scanner at 1.5 Tesla. The method combines a highly stable gradient echo technique with a spiral scan method, to detect brain activation related changes in blood oxygenation with high sensitivity. A motor activation paradigm with a duration of less than 5 min, performed on 10 subjects, consistently showed significant changes in signal intensity in the area of the motor cortex. In all subjects, these changes survived high statistical thresholds.**

**Key words:** MRI, spiral scanning, fMRI, motor cortex.

## INTRODUCTION

Since the introduction of a blood oxygenation level dependent (BOLD) contrast in MRI (1), the number of human brain activation studies employing this contrast has been rapidly growing. Visual and motor cortices were the first (2–5) to be studied with functional MRI (fMRI) techniques. Attempts at studying several other brain areas have followed. However, due to technical difficulties, not all of the studies presented so far have shown reliable mapping of activated regions. Some debate persists about the accuracy of the localization, and whether the observed activation has an intravascular or extravascular origin (6–12). These considerations are crucial for the evaluation of the clinical applicability of fMRI, and for determining its value for important practical applications such as brain mapping, or presurgical planning (13–15).

The success of fMRI scanning methods depends strongly on their ability to discriminate the generally small signal changes related to the activation against a background of changes related to instrumental instabilities and physiologic fluctuations. Poor stability requires an increased number of scans and a lengthening of the activation protocol to reach adequate statistical significance to detect these small signal changes. One approach

to suppress instabilities related to physiologic fluctuations is to reduce the scan time below the time scale of the heart beat and the respiratory cycle, as done using an echo planar imaging (EPI) technique (16). This technique collects a complete scan (one-image slice) in a single pulse repetition (<100 ms). It requires dedicated hardware (fast gradient slew rates), and generally does not allow for single-shot 3D fMRI, but rather a (much slower) slice by slice, or multi-shot 3D (17, 18) scan protocol. On the other hand, fast gradient echo imaging (FGE MRI, also called FLASH, GRASS, or FFE) (19, 20), uses multiple pulse repetitions, requires a longer scan time per image, and can be used with standard clinical MR scanners. It allows both 2D (21, 22) as well as 3D (23, 24) fMRI, although at the cost of a reduced stability as compared with the 2D EPI fMRI methods (2).

Recently, improvements made in FGE fMRI allowed reduction of the number of pulse repetitions required per scan, leading to a reduced scan time (12, 25, 26). This was achieved by an increased coverage of  $k$ -space per  $TR$ . This resulted in an increased number of scans acquired per functional study, and greater statistical power. In particular, spiral FGE techniques (27–29) have attractive characteristics with respect to sensitivity to motion (26, 30–32). In the study presented here, these characteristics are combined with modified gradient schemes and RF phase modulation to develop a 3D spiral FGE MRI technique with minimal sensitivity to physiologic fluctuations.

## METHODS

The following rationale served as a basis for the design of the 3D fMRI scan technique:

- 1: Minimization of gradient moments at acquisition time of the center of  $k$ -space reduces motion-related signal phase instabilities (30–32). This avoids the need of navigator echo-based phase correction (33). Additional stability improvement can be achieved by maintaining constant gradient moments across repetitions (34), in combination with appropriate RF phase modulation schemes (35).
- 2: Spiral scanning allows time-efficient data acquisition by optimum use of gradient capabilities (30) and sampling during ramping of the gradient amplitude. Furthermore, it allows efficient (i.e., circular (36))  $k$ -space coverage.
- 3: 3D scanning reduces the time-of-flight effects (37, 38) experienced by spins moving into the plane under study, thereby avoiding enhancement of in-

MRM 36:620–626 (1996)

From the Laboratory of Diagnostic Radiology Research, OIR, National Institutes of Health (Y.Y., J.A.F., J.H.D.); Department of Diagnostic Radiology, Lucas MRI Center, Stanford University School of Medicine (G.H.G.); In Vivo NMR Research Center, BEIP, NCCRR, National Institutes of Health (P.v.G., C.T.W.M.); Clinical Brain Disorders Branch, NIMH, National Institutes of Health (V.S.M., A.K.S.S., R.H.S., N.F.R., D.R.W.), Bethesda, Maryland.

Address correspondence to: Jeff H. Duyn, Ph.D., Laboratory of Diagnostic Radiology Research, OIR, National Institutes of Health, Building 10, Room B1N-256, Bethesda, MD 20892.

Received December 1, 1995; revised February 7, 1996; accepted May 8, 1996.

0740-3194/96 \$3.00

Copyright © 1996 by Williams & Wilkins

All rights of reproduction in any form reserved.

at 1.5 T

agoda K. S.  
inberger,

biologic fluctua-  
ne time scale of  
s done using an  
This technique  
ce) in a single  
dedicated hard-  
erally does not  
(much slower)  
an protocol. On  
(FGE MRI, also  
uses multiple  
time per image.  
MR scanners. It  
(23, 24) fMRI  
y as compared

fMRI allowed  
ns required per  
, 25, 26). This  
k-space per TR.  
scans acquired  
ical power. In  
have attractive  
to motion (26,  
characteristics  
chemes and RF  
FGE MRI tech-  
ologic fluctua-

or the design of

at acquisition  
motion-related  
his avoids the  
correction (33).  
n be achieved  
oments across  
h appropriate

t data acquisi-  
pabilities (30)  
radient ampli-  
t (i.e., circular

ht effects (37,  
nto the plane  
ncement of in-

travascular spins (8, 9, 23). Furthermore, 3D techniques facilitate image registration procedures.

The pulse diagram for the 3D spiral scan sequence is shown in Fig. 1. The scheme represents gradient and RF waveforms of the sequence. Spiral waveforms of 10 ms were applied on the  $x$  and  $y$  gradients. The waveforms were designed to be slow rate limited except for the first few points, and their maximum amplitude was 0.75 G/cm to give a  $3.8 \times 3.8$  mm nominal in-plane resolution. Six interleaves were measured by adjusting the spiral waveforms (multiplying the  $x$  and  $y$  gradients by coefficients of a rotation matrix) to effectively rotate the  $k$ -space trajectory in the  $k_x$ - $k_y$  plane. At the end of each TR interval, crusher gradients were used to minimize spill-over of FID signal into subsequent TR intervals. Their amplitudes were set to generate about  $3\pi$  dephasing over each voxel dimension. A 65-mm thick slab in the  $z$  (axial) direction was selected in the superior brain, and a 24-step phase encoding cycle was applied in the  $z$  direction. This resulted in a "stacked spirals" (39)  $k$ -space acquisition scheme. The field of view (FOV) in the  $z$  direction was set to 96 mm to render a 4-mm resolution in the axial direction.

With spiral acquisition, all gradient moments:

$$M_n(t) = \int_0^t G(t) \cdot t^n \cdot dt,$$

with  $t = 0$  at the center of the RF pulse, are inherently zero at the center of  $k$ -space ( $t = t_c$ ). The zero<sup>th</sup> ( $M_0(t)$ ) and first ( $M_1(t)$ ) order moments of the slab select gradient were nulled at  $t = t_c$  by using two additional gradient pulses after the slice selection lobe. Furthermore,  $M_0(t)$  for the phase encode gradient and  $M_0(t)$  and  $M_1(t)$  for the spiral waveforms were nulled at  $t = TR$  by additional gradient pulses after the acquisition, to avoid disruption of the steady state by the amplitude changes performed on these gradients on subsequent TR intervals. The gra-

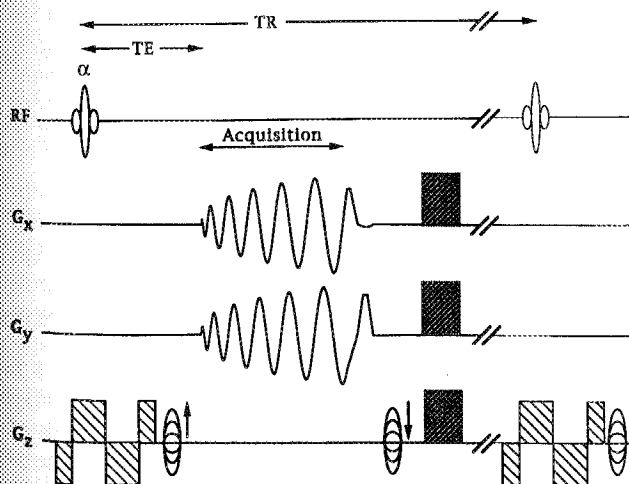


FIG. 1. Pulse sequence for 3D FGE MRI with spiral acquisition, indicating RF pulse and gradient waveforms. On subsequent interleaves, the spiral waveforms were adjusted to effectively rotate the  $k$ -space trajectory in the  $k_x$ - $k_y$  plane.

dient pulses used for nulling the spiral waveforms were composed of trapezoid waveforms of which the amplitudes were adjusted to minimize the gradient moments. For the different interleaves, these moment-nulling gradients were rotated in the  $xy$  plane simultaneously along with the spiral waveforms to maintain the gradient moment compensation. In addition, quadratic RF phase modulation was performed to reduce the contribution of (motion sensitive) stimulated echoes (40). Because linear motion in the presence of the crusher gradient results in a quadratically increasing phase over TR intervals, it could compromise the effectiveness of the phase modulation scheme in suppressing stimulated echoes. Therefore, the optimal choice of the phase increment  $\phi$  of the modulation is critical, and will depend on velocity. For minimal sensitivity to CSF pulsations, a quadratic RF phase modulation scheme was implemented with a phase increment  $\phi$  of  $45^\circ$  (35). Finally, on subsequent 3D scans, the phase encode scheme was inverted to avoid large jumps in gradient moments in subsequent TRs, and therefore to minimize disturbance of the steady state of moving spins.

Experiments were performed on a 1.5 Tesla GE-SIGNA scanner (General Electric, Milwaukee, WI) using the standard GE quadrature head coil and shielded gradients with maximum strength of  $10 \text{ mT} \cdot \text{m}^{-1}$  and maximum slew rate of  $17 \text{ T} \cdot \text{m}^{-1} \cdot \text{s}^{-1}$ . The human subject protocol was approved by the intramural review board of the National Institutes of Health.

Anatomical scans and functional imaging data were acquired from 10 right-handed normal subjects. For the functional scans, the echo time (TE) was 25 ms, and TR was 42 ms. TE was counted from the center of the RF pulse to the start of the acquisition window (center of  $k$ -space). The relatively low value of TE was chosen to allow the short TR of 42 ms, thereby reducing motion sensitivity (31) and increasing the number of scans in the available study time. The RF flip angle (FA) was chosen to be close to the Ernst angle for optimum signal-to-noise ratio ( $16^\circ$ , assuming  $T_1 = 800$  ms for gray matter). The acquisition time for a 3D image was 6 s (6 spiral interleaves, 24 phase encodings). Forty-eight 3D scans were acquired in 288 s, during which the subject switched between rest and finger tapping every 36 s (4 "off-states" and 4 "on-states"). The finger tapping was self-paced (2 Hz) and consisted of sequential thumb-to-digit opposition (in the order of 2, 3, 4, 5, 5, 4, 3, 2) with the dominant (right) hand. Ear plugs were used to reduce noise, and foam packs were applied to restrict head motion.

High resolution (0.5 mm) axial 2D time-of-flight (TOF) images (5 slices, 4 mm in thickness) of the motor cortex were acquired with a spoiled FGE sequence ( $TE/TR = 10/60$  ms,  $FA = 50^\circ$ ) to investigate location and size of the vascular structures. Detailed anatomical structures of the brain including the gray and white matter and small vessels were clearly visible on the TOF images.

Data were processed off line on a Sun-SPARC workstation (Sun Microsystems, Mountain View, CA). For the 3D spiral imaging data, a regridding algorithm was used for reconstruction (41). The spiral scan data were convoluted with a Gaussian window and re-sampled onto a Fourier grid. On the  $k$ -space data, corrections were made

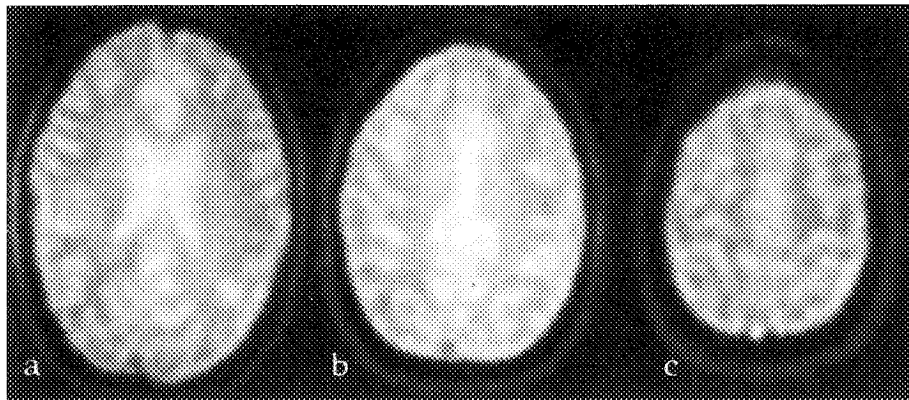


FIG. 2. Subset of images acquired with the spiral sequence ( $TE/TR = 16/30$  ms,  $FA = 5^\circ$ ). Images (a), (b), and (c) are corresponding to three slices (equidistant 12-mm spacing) of a 3D data set (24 slices). Clearly visible are locations of gyri and sulci.

for the non-uniform spiral sampling density. After Fourier transformation, magnitude images were generated, and corrections were made for apodization effects of the convolution window.

All images were registered to the first image to correct for rigid body motion between scans. The registration routine was based on a custom written software package, using a multi-resolution least squares difference algorithm with cubic spline interpolation (42, 43). The functional data were analyzed by means of a  $z$  test adjusted for total number of voxels by using a Bonferroni correction (25). The Bonferroni correction  $\alpha$  level was determined for each individual data set. The total number of voxels in the brain was typically 9500, resulting in an  $\alpha$  level of  $5.3 \times 10^{-6}$  per voxel. Voxels with  $z$  score above 4.41 ( $\alpha$  level 0.05, one sided) were considered as significantly activated (in the following referred to as "activation"). This is a fairly strict selection, since it is equivalent to the occurrence of, on average, one false positive (one voxel incorrectly labeled as active) per 20 subjects. The functional images were overlaid on the TOF images with the aid of a 3D spiral image that showed similar gray/white matter contrasts ( $TE/TR = 16/30$  ms,  $FA = 50^\circ$ ) to the TOF images.

## RESULTS

The 3D spiral images were qualitatively comparable with images obtained with standard FGE MRI with similar

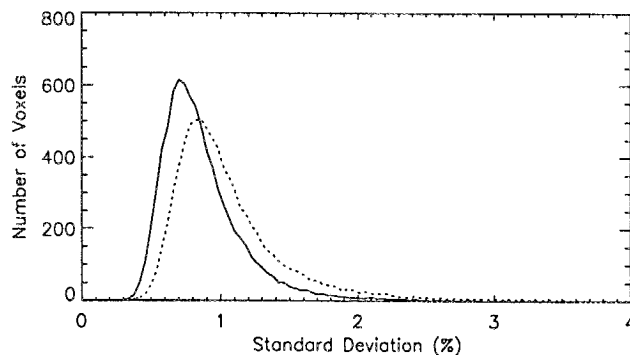


FIG. 3. Histogram of standard deviation over time for all voxels in 3D data. Compared are the new RF phase modulation scheme ( $\phi = 45^\circ$ ) combined with gradient moment nulling (solid line), and conventional RF phase modulation ( $\phi = 117^\circ$ ) with no gradient moment nulling of spiral waveforms (dotted line).

matrix sizes, and similar experimental parameters (24). The reduction of scan time by using spiral readout did not result in visible blurring effects due to  $B_0$  inhomogeneity. Computer simulations showed negligible broadening of the point spread function with  $B_0$  variations of  $\pm 20$  Hz. The spectral line of the signal from the selected brain slab was within 10–20 Hz full width at half maximum (FWHM) in all experiments. In situations where larger  $B_0$  variations are expected, blurring effects could be corrected by postprocessing, using  $B_0$  reference maps (44).

Figure 2 shows a series of images obtained with the 3D spiral technique. The sequence was run at low flip angle ( $FA = 5^\circ$ ) to enhance image contrast and to better appreciate the definition of anatomical details and the scan resolution. Clearly visible in these images are the gyri, sulci, and ventricular spaces. The image resolution is similar to that of standard FGE sequences run with comparable image matrix sizes.

To verify the effectiveness of the pulse sequence design with respect to motion related instabilities, the sequence was run repetitively with the subject in resting state (no finger tapping). As a reference, experiment was repeated with the conventional RF phase modulation scheme ( $\phi = 117^\circ$ ), and without the gradient moment nulling over the repetition time for the spiral waveforms. A comparison of histograms of the voxel standard deviation over acquisition time for both experiments is shown in Fig. 3. On three subjects, the average standard deviation with phase modulation and gradient compensation was  $14 \pm 7\%$  smaller than that without these schemes. The FWHM of the distribution was reduced  $5 \pm 1\%$  with the schemes.

A set of difference images from a single subject, obtained by subtracting the average of "off-states" from the average of "on-states," is displayed in Fig. 4. The high signal intensity voxels in the left hemisphere, representing areas of large signal increases upon activation, were corresponding to locations in the central sulcus, contralateral to the active hand. Note the absence of high signal intensity voxels in other regions, which display more or less uniform noise. Figure 5 shows the result of the statistical analysis, for slices 14–17 of Fig. 4, demonstrating the significant signal changes are predominantly located in primary sensorimotor cortex regions. Some of the activated voxels overlap small vessels. An example of the time course of a single voxel within an activated motor cortex is shown in Fig. 6. A composite histogram

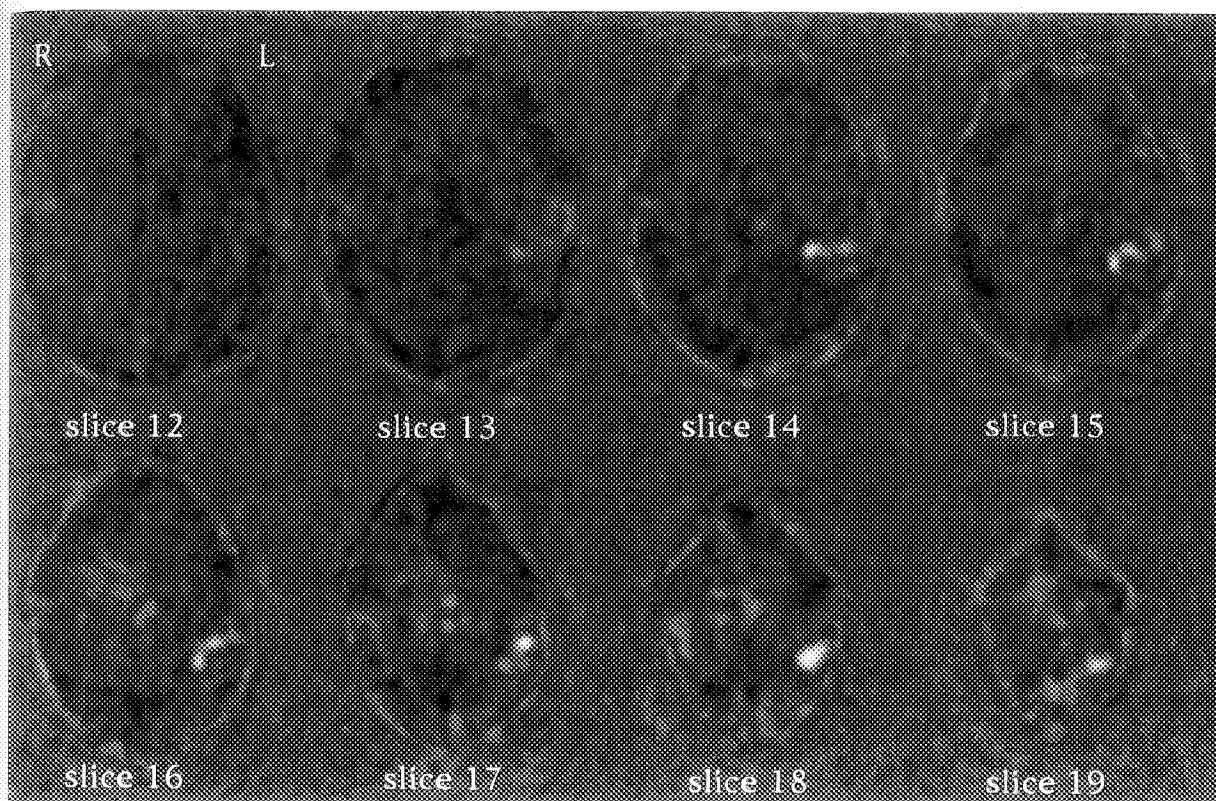


FIG. 4. Difference images, obtained from 3D spiral motor cortex activation study. Displayed is a selection of 8 out of 24 slices, from a region encompassing the motor cortex. Bright image intensities correspond to signal increases. Note the focal signal increase in the left hemisphere (L), as compared with a virtual absence of signal changes in the right hemisphere (R).

of percentage activation of all the voxels surviving the  $z$  threshold from all 10 subjects is shown in Fig. 7. Among the subjects, the magnitude of the signal increase in activated voxels ranged from 0.8–5.0% (mean 1.8% and standard deviation 0.6%).

Locations and volumes of the activated areas of the 10 subjects are summarized in Table 1. Activated voxels were counted in regions of interest (ROIs), selected *a priori* on anatomical images. The extents of the motor regions were defined as follows: 1) primary sensorimotor cortex (PSM)—area encompassing the central sulcus, including the posterior half of the precentral gyrus and anterior half of the post central gyrus; 2) supplementary motor area (SMA)—area anterior to the mesial aspect of the precentral gyrus. All of the subjects showed activation in the left motor cortex. Most of the activated volume was located in the left PSM, whereas less activation was observed in the SMA and other, unidentified areas.

## DISCUSSION

The excellent stability of the 3D spiral technique, as evidenced by the uniformity of the noise in the difference images (Fig. 4), as well as its consistency to detect activation with relatively little data (i.e., <5 min) can be attributed to the following factors. First, the more efficient  $k$ -space coverage with spiral trajectories allowed for reduction of the scan time, leading to reduction of phase fluctuations during a single scan, and allowing more scans to be acquired in the same total study time. Be-

cause magnitude images were used in statistical analysis, phase fluctuations of the MR signal across scans did not affect the results. Secondly, there are reduced phase fluctuations at the center of  $k$ -space, because of the absence of moments of the imaging gradients, and because of the averaging of multiple acquisition of this center, inherent to interleaved spiral imaging (31). Phase fluctuations were further reduced by gradient moment nulling of the slice select waveform. Finally, additional 14% stability improvement was achieved by gradient moment nulling over the entire  $TR$  and the use of a quadratic phase modulation scheme with  $\phi = 45^\circ$  (35).

The results of the functional studies on 10 subjects show a very consistent activation of the motor cortex. All subjects showed increased signal in the primary sensorimotor cortex. Less consistent was the activation in the supplementary motor area, confirming earlier fMRI studies (25). Averaged over all subjects, only 12.8% of the activated voxels were outside the PSM and SMA. The mean percentage activation within voxels with  $z$  scores above threshold was 1.82%, which, after correction for differences in  $TE$ , corresponds to previous results from BOLD-sensitized FGE (25) and EPI (2) techniques. Some voxels showed larger activation (up to 5% signal increase), inconsistent with a BOLD effect originating solely from the capillary bed. Comparison with the high resolution TOF maps indicated that most of these voxels were suspect for involvement of the larger veins. This was also the case for some of the voxels with lower signal

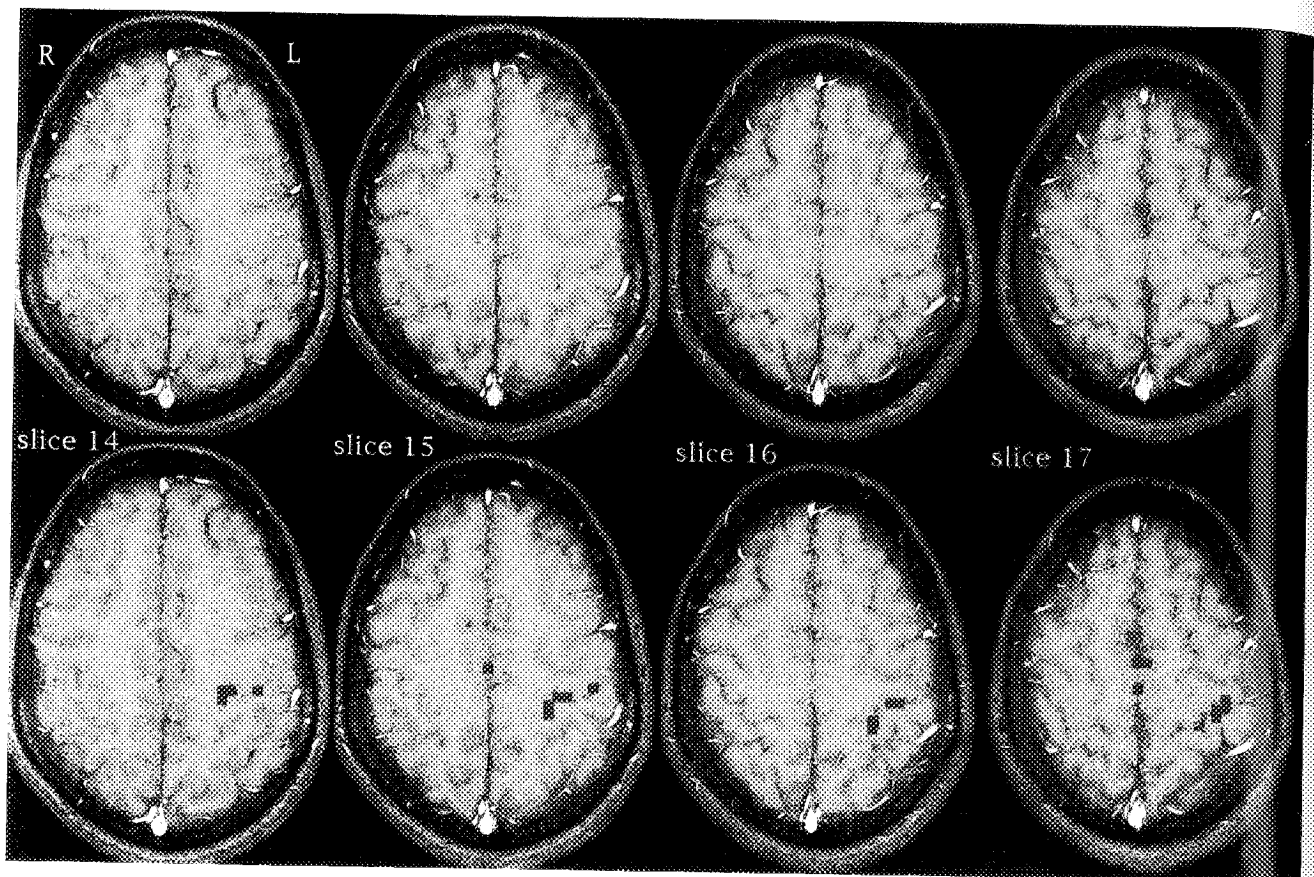


FIG. 5. Time-of-flight images of slices 14–17 of Fig. 4 (top row), together with an overlay of the functional maps on these images (bottom row). Note the focal activation observed in the left primary sensorimotor cortex, and the supplementary motor area.

increases. The large percentage activation could be caused by a BOLD effect either within or around these vessels (45). This suggests that caution has to be exercised when interpreting the results, since, for example, draining veins could show activation quite remote from the activated cortex (8). Further investigations are necessary to discriminate capillary involvement against contributions from the larger veins. This could be facilitated by increasing the spatial and/or temporal resolution (12) using the faster gradient switching systems currently being introduced to clinical MRI scanners.

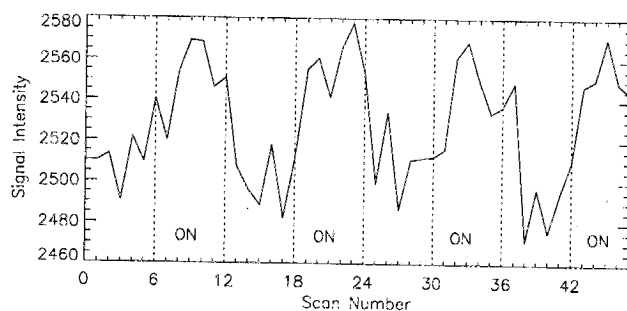


FIG. 6. An example of the signal time course of the functional data from a single voxel in the motor cortex region. Signal increases correlating with the activation paradigm are easily discernible above the noise fluctuations.

## CONCLUSION

We have developed a fast 3D spiral imaging sequence for functional studies of human brain. A BOLD-sensitized 3D image can be acquired in 6 s. High signal stability was achieved by gradient moment nulling and modified RF phase modulation. Motor cortex activation studies on a standard clinical 1.5 T scanners consistently detected

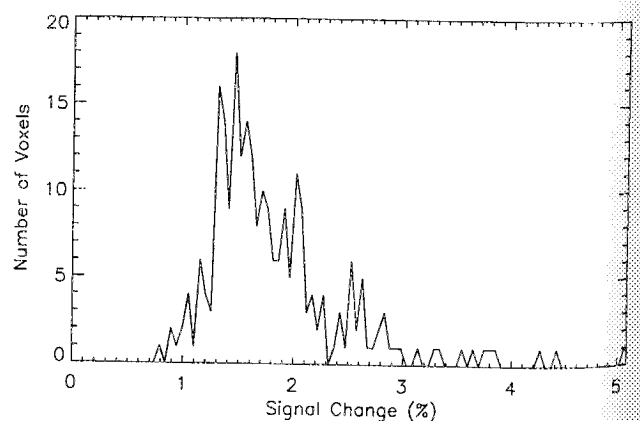


FIG. 7. Composite histogram of percentage activation of all the activated voxels obtained from all 10 subjects. A peak in the occurrence is observed around 1.6% signal increase, with a mean of 1.8% and a standard deviation 0.6%.

**Table 1**  
**Volumes (ml) of Significant Activation ( $z > 4.41$ ) in PSM and SMA, and Percentages of Combined Volumes of PSM and SMA in the Total Activation Volumes**

Volunteer	Total	PSM	SMA	(PSM+SMA)/Total (%)
1	2.31	1.60	0.53	92.7
2	1.81	1.54	0.17	94.6
3	1.20	0.75	0.31	88.2
4	2.32	1.65	0.25	81.8
5	0.45	0.42		93.8
6	1.98	1.63	0.13	88.7
7	0.25	0.18		72.2
8	1.56	1.10	0.06	73.8
9	1.20	1.01	0.06	89.4
10	0.80	0.69	0.08	96.5
Mean	1.39	1.05	0.16	87.2
SD	0.74	0.54	0.17	8.5

activation in the expected area, with a study time of less than 5 min.

## REFERENCES

- S. Ogawa, T. M. Lee, A. S. Nayak, P. Glynn, Oxygenation-sensitive contrast in magnetic resonance imaging of rodent brain at high magnetic fields. *Magn. Reson. Med.* **14**, 68-78 (1990).
- K. K. Kwong, J. W. Belliveau, D. A. Chesler, I. E. Goldberg, R. M. Weiskoff, B. P. Poncelet, D. N. Kennedy, B. E. Hoppel, M. S. Cohen, R. Turner, H. Cheng, T. J. Brady, B. R. Rosen, Dynamic magnetic resonance imaging of human brain activity during primary sensory stimulation. *Proc. Natl. Acad. Sci. USA* **89**, 5675-5679 (1992).
- P. A. Bandettini, E. C. Wong, R. S. Hinks, R. S. Tikofsky, J. S. Hyde, Time course EPI of human brain function during task activation. *Magn. Reson. Med.* **25**, 390-397 (1992).
- S. G. Kim, J. Ashe, A. P. Georgopoulos, H. Merkle, J. M. Ellermann, R. S. Menon, S. Ogawa, K. Ugurbil, Functional imaging of human motor cortex at high magnetic field. *J. Neurophysiol.* **69**, 297-302 (1993).
- S. M. Rao, J. R. Binder, P. A. Bandettini, T. A. Hammel, F. Z. Yetkin, A. Jesmanowicz, L. M. Lisk, C. L. Morris, W. M. Mueller, L. D. Estkowski, E. C. Wong, V. M. Haughton, J. S. Hyde, Functional magnetic resonance imaging of complex human movements. *Neurology* **43**, 2311-2318 (1993).
- P. A. Bandettini, E. C. Wong, A. Jesmanowicz, R. S. Hinks, J. S. Hyde, Spin-echo and gradient-echo EPI of human brain activation using BOLD contrast: a comparative study at 1.5 T. *NMR Biomed.* **7**, 12-20 (1994).
- J. L. Boxerman, P. A. Bandettini, K. K. Kwong, J. R. Baker, T. L. Davis, B. R. Rosen, R. M. Weiskoff, The intravascular contribution to fMRI signal change: Monte Carlo modeling and diffusion-weighted studies in vivo. *Magn. Reson. Med.* **34**, 4-10 (1995).
- J. H. Duyn, C. T. W. Moonen, G. H. van Yperen, R. W. de Boer, P. R. Luyten, Inflow versus deoxyhemoglobin effects in 'BOLD' functional MRI using gradient echoes at 1.5 T. *NMR Biomed.* **7**, 83-88 (1994).
- S. Gromiscek, R. Beisteiner, K. Hittmair, E. Mueller, E. Moser, A possible role of in-flow effects in functional MR imaging. *Magn. Reson. Mater. Phys. Biol. Med.* **1**, 109-113 (1993).
- S. Lai, A. L. Hopkins, E. M. Haacke, D. Li, B. A. Wasserman, P. Buckley, L. Friedman, A. Metzler, P. Hedera, R. Friedland, Identification of vascular structures as a major source of signal contrast in high resolution 2D and 3D functional activation imaging of motor cortex at 1.5 T: preliminary results. *Magn. Reson. Med.* **30**, 387-392 (1993).
- S. G. Kim, K. Hendrich, X. Hu, H. Merkle, K. Ugurbil, Potential pitfalls of functional MRI using conventional gradient-recalled echo techniques. *NMR Biomed.* **7**, 69-74 (1994).
- A. T. Lee, G. H. Glover, C. H. Meyer, Discrimination of large venous vessels in time-course spiral blood-oxygen-level-dependent magnetic-resonance functional neuroimaging. *Magn. Reson. Med.* **33**, 745-754 (1995).
- Y. Cao, V. L. Towle, D. N. Levin, R. Grzeszczuk, J. F. Mullan, Conventional 1.5 T functional MRI localization of human hand sensorimotor cortex with intraoperative electrophysiologic validation, in "Proc., SMRM, 12th Annual Meeting, New York, 1993," p. 1417.
- R. Howard, D. Alsop, J. Detre, Functional MRI of regional brain activity in patients with intracerebral gliomas and AVMs prior to surgical or endovascular therapy, in "Proc., SMR, 2nd Annual Meeting, San Francisco, 1994," p. 701.
- C. R. Jack Jr., R. M. Thompson, R. K. Butts, F. W. Sharbrough, P. J. Kelly, D. P. Hanson, S. J. Riederer, R. L. Ehman, N. J. Hangiandreou, G. Cascino, Sensory motor cortex: correlation of presurgical mapping with functional MR imaging and invasive cortical mapping. *Radiology* **190**, 85-92 (1994).
- P. Mansfield, I. Pykett, Biological and medical imaging by NMR. *J. Magn. Reson.* **29**, 355-373 (1978).
- P. Mansfield, A. M. Howseman, R. J. Ordidge, Volumar imaging using NMR spin echoes: echo-volumar imaging (EVI) at 0.1 T. *J. Phys. E.* **22**, 324-330 (1989).
- M. S. Cohen, M. L. Rohan, 3D volume imaging with instant scan, in "Proc., SMRM, 8th Annual Meeting, Amsterdam, The Netherlands, 1989," p. 831.
- A. Haase, J. Frahm, D. Matthaei, W. Haenicke, K. D. Merboldt, Flash imaging. Rapid NMR imaging using low flip angle pulses. *J. Magn. Reson.* **67**, 217-225 (1986).
- P. van der Meulen, J. P. Groen, J. J. M. Cuppen, Very fast MR imaging by field echoes and small angle excitation. *Magn. Reson. Imaging* **3**, 297-299 (1985).
- S. Ogawa, D. W. Tank, R. Menon, J. M. Ellermann, S. G. Kim, H. Merkle, K. Ugurbil, Intrinsic signal changes accompanying sensory stimulation: functional brain mapping with magnetic resonance imaging. *Proc. Natl. Acad. Sci. USA* **89**, 5951-5955 (1992).
- J. Frahm, H. Bruhn, K. Merboldt, W. Hanicke, Dynamic MR imaging of human brain oxygenation during rest and photic stimulation. *J. Magn. Reson. Imaging* **2**, 501-505 (1992).
- J. H. Duyn, V. S. Mattay, R. H. Sexton, G. S. Sobering, F. A. Barrios, G. Liu, J. A. Frank, D. R. Weinberger, C. T. W. Moonen, 3-Dimensional functional imaging of human brain using echo-shifted FLASH MRI. *Magn. Reson. Med.* **32**, 150-155 (1994).
- L. R. Schad, F. Wenz, M. V. Knopp, K. Baudendistel, E. Mueller, W. J. Lorenz, Functional 2D and 3D magnetic resonance imaging of motor cortex stimulation at high spatial resolution using standard 1.5 T imager. *Magn. Reson. Imaging* **12**, 9-15 (1994).
- P. van Gelderen, N. F. Ramsey, G. Liu, J. H. Duyn, J. A. Frank, D. R. Weinberger, C. T. W. Moonen, Three-Dimensional functional magnetic resonance imaging of human brain on a clinical 1.5-T scanner. *Proc. Natl. Acad. Sci. USA* **92**, 6906-6910 (1995).
- D. C. Noll, J. D. Cohen, C. H. Meyer, W. Schneider, Spiral k-space MR imaging of cortical activation. *J. Magn. Reson. Imaging* **5**, 49-56 (1995).
- R. S. Likes, Moving gradient Zeugmatography. U. S. Patent 4307343 (1981).
- S. Ljungren, A simple graphical representation of Fourier-based imaging methods. *J. Magn. Reson.* **54**, 338-343 (1983).
- C. B. Ahn, J. H. Kim, Z. H. Cho, High-speed spiral-scan echo planar NMR imaging. *IEEE Trans. Med. Imaging* **5**, 2-7 (1986).
- C. H. Meyer, B. S. Hu, D. G. Nishimura, A. Macovski, Fast spiral coronary artery imaging. *Magn. Reson. Med.* **28**, 202-213 (1992).
- G. H. Glover, A. T. Lee, Motion artifacts in fMRI: Comparison of 2DFT with PR and spiral scan methods. *Magn. Reson. Med.* **33**, 624-635 (1995).
- D. G. Nishimura, P. Irarrazabal, C. H. Meyer, A velocity k-space analysis of flow effects in echo-planar and spiral imaging. *Magn. Reson. Med.* **33**, 549-556 (1995).
- R. L. Ehman, J. P. Felmler, Adaptive technique for high-definition MR imaging of moving structures. *Radiology* **173**, 255-263 (1989).
- Y. Zur, M. L. Wood, L. J. Neuringer, Motion-insensitive, steady-state free precession imaging. *Magn. Reson. Med.* **16**, 444-459 (1990).
- J. H. Duyn, Steady state effects in fast gradient echo imaging, in "Proc. SMR, 4th Annual Meeting, New York, 1996," p. 1473.
- A. A. Maudsley, G. B. Matson, J. W. Hugg, M. W. Weiner, Reduced phase encoding in spectroscopic imaging. *Magn. Reson. Med.* **31**, 645-51 (1994).
- G. T. Gullberg, F. W. Wehrli, A. Shimakawa, M. A. Simons, MR

se images (bottom

ng sequence for  
 OLD-sensitized  
 al stability was  
 and modified RF  
 on studies on a  
 tently detected



activation of all the  
 ts. A peak in the  
 rease, with a mean

- vascular imaging with a fast gradient refocusing pulse sequence and reformatted images from transaxial sections. *Radiology* **165**, 241-246 (1987).
38. J. H. Gao, S. K. Holland, J. C. Gore, Nuclear Magnetic Resonance signal from nuclei in rapid imaging using gradient echoes. *Med. Phys.* **15**, 809-814 (1988).
  39. P. Irarrazabal, D. G. Nishimura, Fast three dimensional magnetic resonance imaging, *Magn. Reson. Med.* **33**, 656-662 (1995).
  40. Y. Zur, M. L. Wood, L. J. Neuringer, Spoiling of transverse magnetization in steady-state sequences. *Magn. Reson. Med.* **21**, 251-263 (1991).
  41. J. I. Jackson, C. H. Meyer, D. G. Nishimura, A. Macovski, Selection of a convolution function for Fourier inversion using gridding. *IEEE Trans. Med. Imaging* **10**, 473-478 (1991).
  42. M. Unser, A. Aldroubi, A multiresolution image registration procedure using spline pyramids, in "Proc., SPIE, San Diego, California, U.S.A., 1993, vol. 2034, Mathematical Imaging: Wavelet Applications in Signal and Image Processing," pp. 160-170.
  43. P. Thevenaz, U. E. Ruttimann and M. Unser, Iterative multi-scale registration without landmarks, in "Proc., International Conference on Image Processing, Washington, D.C., U.S.A., 1995, vol. III," pp. 228-231.
  44. D. C. Noll, C. H. Meyer, J. M. Pauly, D. G. Nishimura, A. Macovski, A homogeneity correction method for magnetic resonance imaging with time-varying gradients. *IEEE Trans. Med. Imaging* **10**, 629-637 (1991).
  45. J. H. Duyn, N. R. Ramsey, V. S. Mattay, P. van Gelderen, C. T. W. Moonen, R. H. Sexton, K. A. Tallent, D. R. Weinberger, J. A. Frank, Effects of large vessels in functional magnetic resonance imaging at 1.5 Tesla. *Int. J. Imaging Syst. Technol.*, **6**, 245-257 (1995).

The  
wat  
tion  
the  
diff  
coe  
atte  
1.7  
sciz  
dege  
diffu  
in d  
axo  
micr  
Key  
gene

INTE  
The  
wat  
and  
{1-7  
nerv  
The  
mult  
seco  
verse  
mark  
that  
the a  
to est  
micr  
ciatic  
must  
diffu  
other

MRM 3  
From  
Edmon  
Address  
ical Eng  
Edmont  
Receive  
The wo  
ership  
postgra  
Medical  
0740-31  
Copyrig  
All right